ACCOUNTS of chemical research

pubs.acs.org/accounts Article

Interplay of Phonon Directionality and Emission Polarization in Two-Dimensional Layered Metal Halide Perovskites

Roman Krahne,* Miao-Ling Lin, and Ping-Heng Tan

Cite This: *Acc. Chem. Res.* 2024, 57, 2476−2489 Read Online

CONSPECTUS: Layered metal halide perovskites represent a natural quantum well system for charge carriers that provides rich physics, and the organic encapsulation of the inorganic metal halide layers not only increases their stability in devices but also provides an immense freedom to design their functionality. Intriguingly, these organic moieties strongly impact the optical, electrical, and mechanical properties, not only through their dielectric, elastic, and chemical properties but also because of induced mechanical distortions in the inorganic lattice. This tunability makes two-dimensional layered perovskites (2DLPs) highly attractive as light emitters. Common consensus is that exciton−phonon coupling plays an important role in radiative recombination. For bulk and some two-dimensional (2D) materials, the band edge emission broadening can be described by the classic models for polar inorganic semiconductors, while for the temperature dependence of the self-trapped exciton emission, an analysis developed for color centers has been successfully applied. For many 2DLPs these approaches do not work because of the complexity of their vibrational spectra. However, their emission is still strongly determined by phonons, and therefore, an adequate understanding of the electron−phonon coupling needs to be developed.

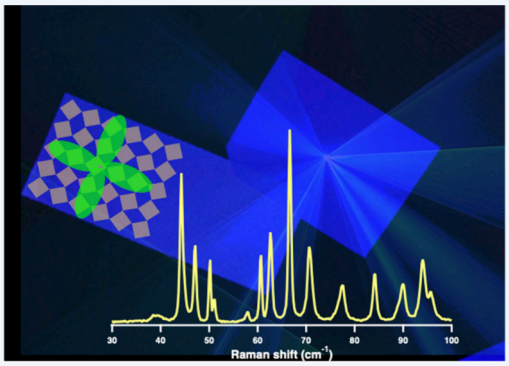

With polarized and angle-resolved Raman spectroscopy studies on single 2DLP flakes based on different ammonium molecules as organic cations, in 2020 we revealed very rich phonon spectra in the low-frequency regime. Although the phonon bands at low frequency can generally be attributed to the vibrations of the inorganic lattice, we found very different responses by only changing the type of organic cations. In addition, the intensity of the different phonon modes depended strongly on the angle of the linearly polarized excitation beam with respect to the in-plane axes of the octahedron lattice. In 2022, we mapped this angular dependence of the phonon modes, which allowed identification of the directionality of the different lattice vibrations. By correlating the phonon spectra with the temperature-dependent emission for a set of 2DLPs that featured very different self-trapped exciton (STE) emission, we demonstrated that the exciton relaxation cannot be related to coupling with a single (longitudinal-optical) phonon band and that several phonon bands should be involved in the emission process. To gain insights into the exciton−phonon coupling effects on the band edge emission, we performed both angle-resolved polarized emission and Raman spectroscopy on single 2D lead iodide perovskite microcrystals. These experiments revealed the impact of the organic cations on the linear polarization of the emission and corroborated that multiple phonon bands should be involved in the radiative recombination process. Analysis of the temperature-dependent line width broadening of the band edge emission showed that for many systems, the behavior cannot be described by assuming the involvement of only one phonon mode in the electron−phonon coupling process. Our studies revealed a wealth of highly directional low-frequency phonons in 2DLPs from which several bands are involved in the emission process, which leads to diverse optical and vibrational properties depending on the type of organic cation in the material.

KEY REFERENCES

- Dhanabalan, B.; Leng, Y.-C.; Biffi, G.; Lin, M.-L.; Tan, P.-H.; Infante, I.; Manna, L.; Arciniegas, M. P.; Krahne, R. Directional Anisotropy of the Vibrational Modes in 2D-Layered Perovskites. *ACS Nano* **2020**, *14*, 4689−4697.[1] *This work used Raman spectroscopy and density functional theory to analyze the complex vibrational response of 2DLP single crystals with different organic cations. Polarized Raman spectroscopy revealed that the phonon spectra depend strongly on the crystal orientation.*
- Lin, M.-L.; Dhanabalan, B.; Biffi, G.; Leng, Y.-C.; Kutkan, S.; Arciniegas, M. P.; Tan, P.-H.; Krahne, R. Correlating Symmetries of Low-Frequency Vibrations

Received: May 2, 2024
Revised: August 7, 2024
Accepted: August 7, 2024
Published: August 21, 2024

https://doi.org/10.1021/acs.accounts.4c00259
Acc. Chem. Res. 2024, 57, 2476−2489

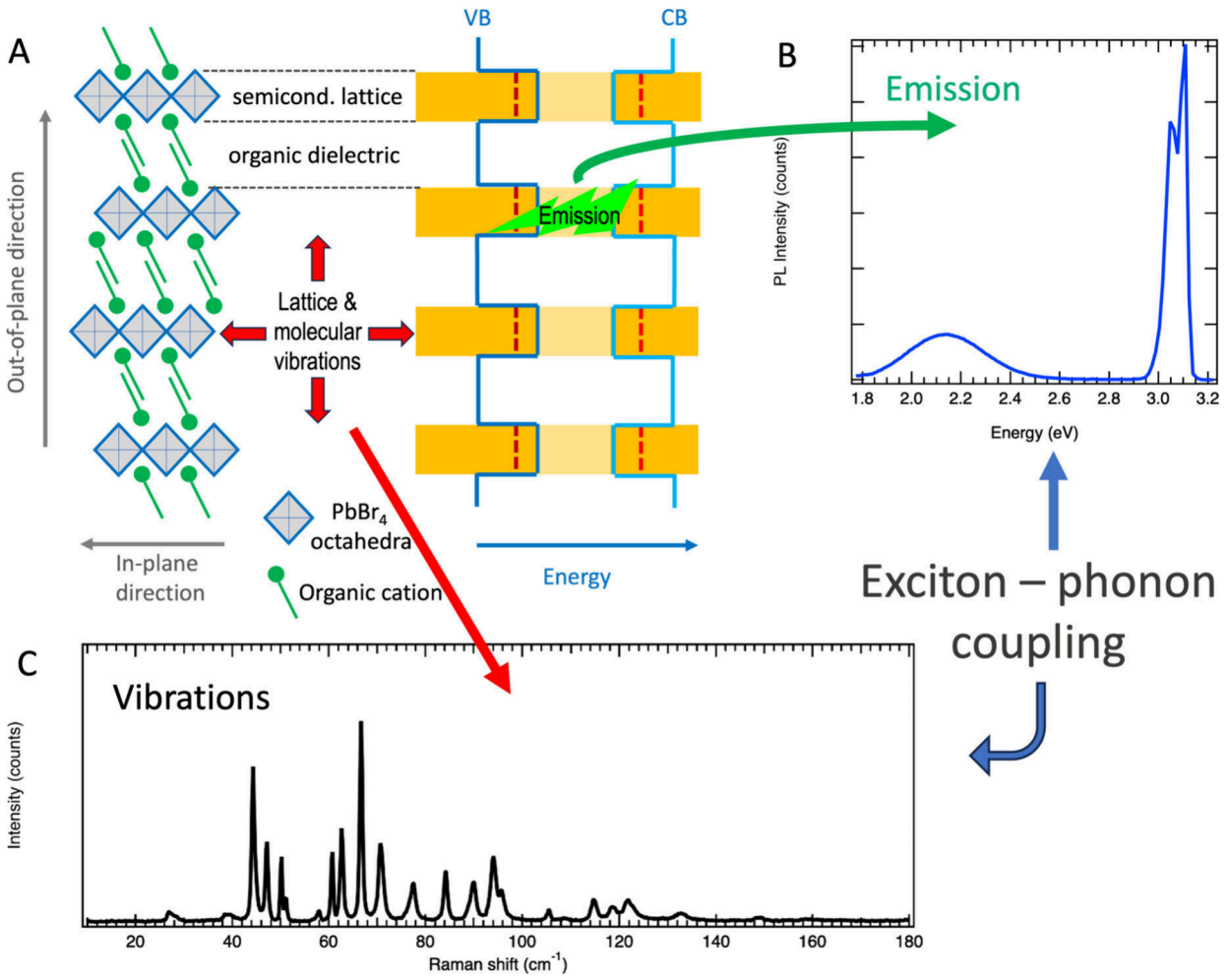

Figure 1. Two-dimensional metal halide perovskites: architecture and typical emission and vibration spectra. (A) Schematic illustration of the organic−inorganic layered structure that results in a periodic lattice of quantum wells in the vertical direction. (B, C) Emission and Raman spectra recorded at cryogenic temperatures from single exfoliated $(UDA)_2PbBr_4$ flakes. Adapted from ref 2. CC BY-NC 4.0.

and Self-Trapped Excitons in Layered Perovskites for Light Emission with Different Colors. *Small* **2022**, *18*, 2106759.[2] *Here we assigned the directionality of the vibrational motion of the different phonon bands using angle-resolved polarized Raman spectroscopy. Studying 2DLPs with strong broadband emission evidenced the shortcomings of electron−phonon coupling analysis based on a single phonon mode.*

- Martín-García, B.; Spirito, D.; Lin, M.-L.; Leng, Y.-C.; Artyukhin, S.; Tan, P.-H.; Krahne, R. Low-Frequency Phonon Modes in Layered Silver−Bismuth Double Perovskites: Symmetry, Polarity, and Relation to Phase Transitions. *Adv. Opt. Mater.* **2022**, *10*, 2270056.[3] *In this work we investigated lead-free double perovskites with different dimensionalities by angle-resolved Raman spectroscopy and provided a detailed microscopic and group theory assignment of the Raman modes. With temperature-dependent measurements we revealed first- and second-order phase transitions.*
- Krahne, R.; Schleusener, A.; Faraji, M.; Li, L.-H.; Lin, M.-L.; Tan, P.-H. Phonon Directionality Impacts Electron-Phonon Coupling and Polarization of the Band-Edge Emission in Two-Dimensional Metal Halide Perovskites. *Nano Lett.*, 10.1021/acs.nanolett.4c03543.[4] *In this study we investigated lead iodide 2DLP microcrystals with angle-resolved polarized photoluminescence and Raman spectroscopy, which allowed us to directly correlate the directional properties of the phonons to the angle-dependent polarization of the band edge emission.*

1. INTRODUCTION

Materials science is evolving toward increasingly complex structures that combine the properties of several different components in composites,[5] self-assembled structures of different dimensions,[6−8] and other architectures.[9] In this respect, hybrid organic−inorganic metal halide perovskites have recently gained strong interest as extremely versatile platforms that combine the optoelectronic properties of solid-state matter with the softness, flexibility, and huge variety of organic molecules.[10−12] Following their astonishing success in solar cells,[13] these materials also proved to be highly versatile in light emission, optoelectronics, and other fields.[14] Low-dimensional metal halide perovskites[15,16] evolved from the bulk materials by the introduction of organic species that are too large to fit into the voids of the octahedron lattice. With such large organic cations, typically consisting of an amine headgroup that binds to the metal halide octahedra and an aliphatic chain or aromatic ring as a backbone, layered structures can be achieved that consist of alternating inorganic

https://doi.org/10.1021/acs.accounts.4c00259
Acc. Chem. Res. 2024, 57, 2476−2489

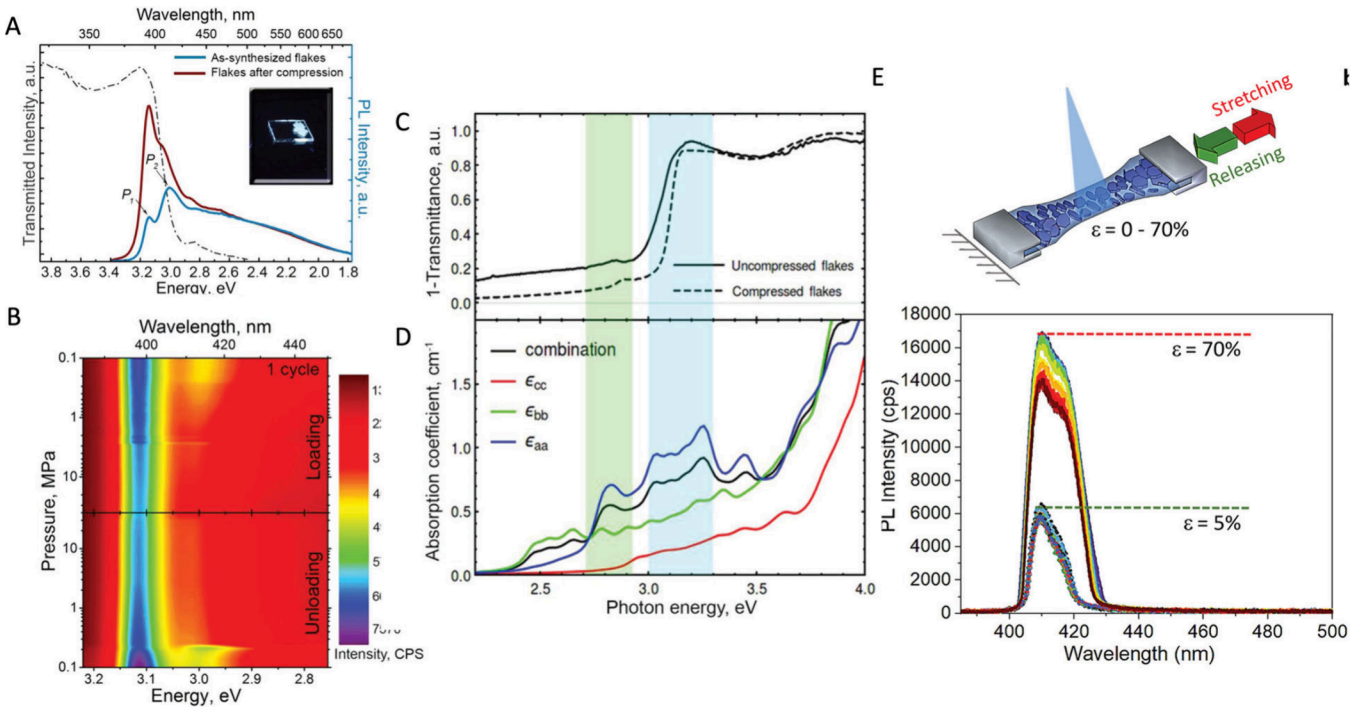

Figure 2. Emission tunability of 2DLP ensembles by stress-induced alignment of the microcrystals. (A, B) Change of the photoluminescence (PL) spectrum under compression of the ensemble by applying pressures in the MPa range. (C) Calculated transmittance of the microcrystal ensemble with and without compression. (D) Simulated absorption along the crystallographic directions, where ϵ_{aa}, ϵ_{bb}, and ϵ_{cc} are the diagonal elements of the dielectric tensor, and *a*, *b*, and *c* are the crystallographic axes of the structure with the octahedron lattice in the *ab* plane. Reproduced with permission from ref 53. Copyright 2018 Wiley-VCH. (E) Illustration of the stretchable PDMS film loaded with 2DLP microcrystals and emission spectra for various cycles under 5% and 70% stretch. Reproduced from ref 57. CC BY-NC 3.0.

octahedron lattices and organic layers,[17] as illustrated in Figure 1A. Controlling the number (n) of adjacent octahedra in the vertical direction in the inorganic layer by the ratio of large to small organic cations in the synthesis provides a handle to tune the confinement of the electrical carriers in the semiconducting layer from quasi-bulklike (large n) to two-dimensional (2D) with small n.[18−20] With only one ammonium species, purely 2D crystals (n = 1) are obtained that are the subject of this Account, for which we consider the Ruddlesden−Popper phase that features a tail-to-tail connection of the organic cations at the center of the organic layer that leads to a van der Waals gap.[21] This architecture allows for a very large freedom in the choice of the organic molecules that can be employed to design their structural and optoelectronic properties[22−24] and favors the mechanical exfoliation of thin flakes from larger crystals.[25] Low-dimensional metal halide perovskites combine inorganic (metal halide octahedron) lattices that can be described by band structure physics and collective lattice vibrations (phonons) with organic materials whose behavior is governed by molecular orbitals and vibrations of chemical bonds. Building on the extensive knowledge on solid-state 2D materials, their optical and elastic properties are typically described in terms of electronic bands and optical and acoustic phonon modes.[26−29] In particular, the analysis of electron−phonon coupling,[30] considering longitudinal-optical (LO) phonons and Fröhlich coupling, has been applied to describe the emission line width broadening in 2D layered perovskites (2DLPs), in analogy to inorganic (nano)crystal materials.[28,31−33] However, the vibrational response, or phonon spectrum, of 2DLPs can consists of a very large number of phonon bands, where the identification of a single phonon mode that governs the electron−phonon coupling is not possible.[2,34] Therefore, such analysis can yield, at best, reasonable average values for the phonon energies and coupling strengths that contribute to the emission broadening. Our studies on the low-frequency vibrational properties and temperature-dependent emission of 2DLPs evidenced the limits of such a solid-state analysis of the electron−phonon coupling,[2,35] which is one focus of the discussion in this Account. Furthermore, we will give a comprehensive overview of the directionality of the phonon modes with respect to the axes of the octahedron lattice based on our angle-resolved polarized Raman spectroscopy experiments, where we investigated 2DLPs with different halides and different metal and organic cations.[1−4]

2. TWO-DIMENSIONAL LAYERED PEROVSKITES: EMISSION AND VIBRATION PROPERTIES

The layered 2D perovskite architecture resembles stacks of semiconductor quantum wells separated by dielectric layers formed by the organic molecules, as illustrated in Figure 1. This very sophisticated structure has many particular features: (i) it is strongly anisotropic, with quasi-infinite in-plane extension and strong vertical confinement of the order of 1 nm; (ii) it combines the elastic properties of the inorganic octahedron lattice (that can be described in terms of acoustic and optical phonons) with those of the organic layer, where vibrations originate from the molecular bonds; (iii) the overall lattice structure is relatively soft, and therefore, deformations can be easily induced by steric hindrance or electrical charges; (iv) the energy levels and electronic band structure depend on both the composition of the metal halide lattice and the species of organic cations.

https://doi.org/10.1021/acs.accounts.4c00259
Acc. Chem. Res. 2024, 57, 2476−2489

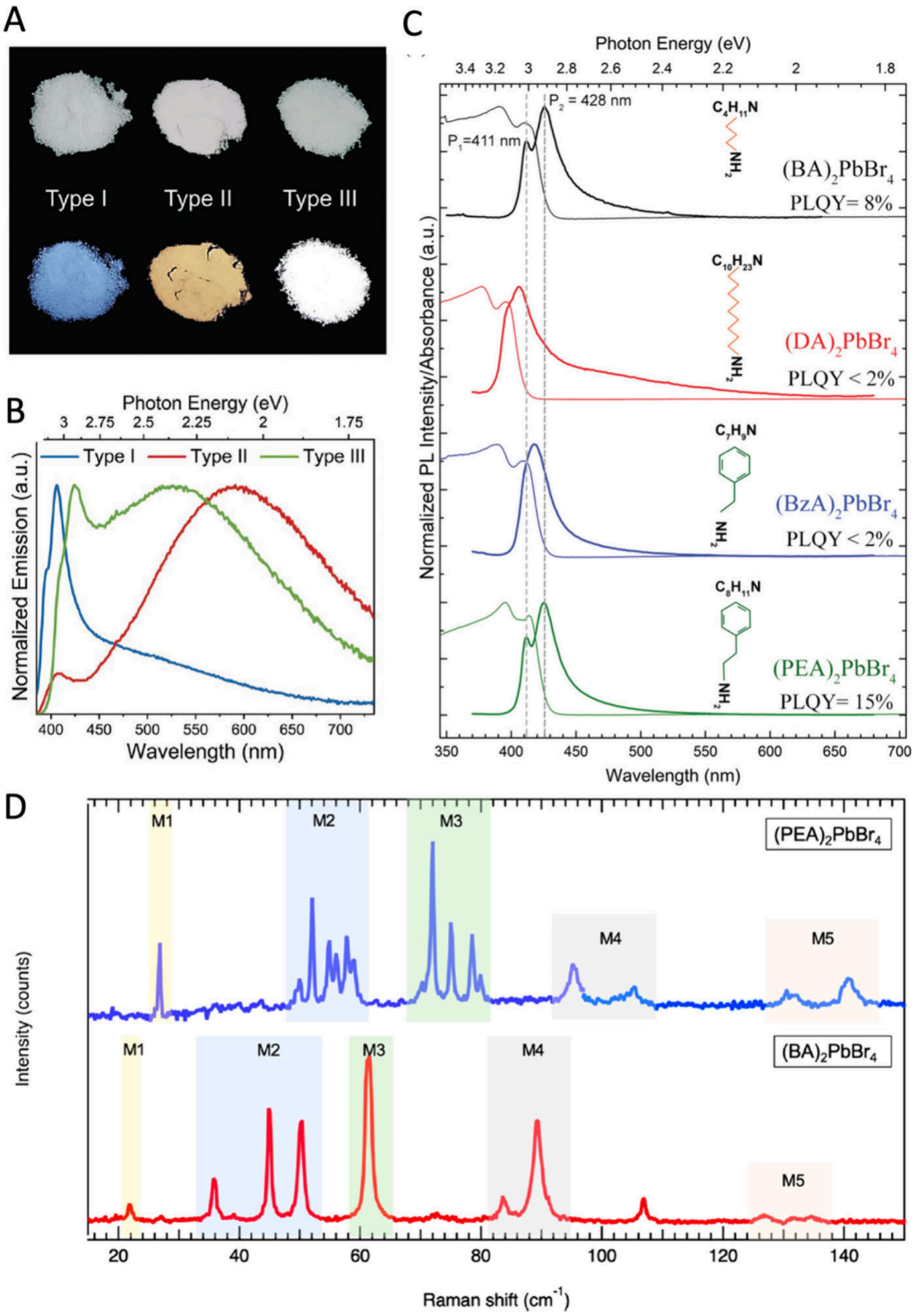

Figure 3. Exciton and phonon bands of 2D lead bromide perovskites with different organic phases. (A, B) 2D perovskite powders with organic cations that have different amine bonding groups under (top) daylight and (bottom) UV light, showing different colors (A) and emission spectra (B). Reproduced from ref 43. CC BY 4.0. (C) Emission and absorption spectra recorded from powders of 2D perovskites with different primary ammonium cations. Reproduced from ref 58. CC BY-NC 3.0. (D) Raman spectra of 2D perovskites with different primary ammonium cations recorded at cryogenic temperatures, where phonon bands attributed to similar vibration modes are highlighted by the shaded background. Reproduced from ref 1. Copyright 2020 American Chemical Society.

Accordingly, such materials feature much more complex optical and elastic spectra compared to purely inorganic solid-state crystals, as shown in Figure 1B,C. The emission spectrum (Figure 1B) typically consists of a set of several peaks stemming from free excitons at the band edge, where the energy level structure depends on spatially diverse confinement effects[36−38] and lattice asymmetries caused by distortions.[39,40] Furthermore, often a broad emission band at lower energy is observed that is related to self-trapped excitons (STEs) or defects.[28,41−44] Concerning the elastic properties, 2DLPs feature a very large number of vibrational modes or phonon bands, as shown in the Raman spectrum in Figure 1C. These

https://doi.org/10.1021/acs.accounts.4c00259
Acc. Chem. Res. 2024, 57, 2476−2489

modes can be associated different kinds of oscillations, such as octahedron rocking or twisting, metal−halide bond bending or stretching, coupled modes involving the organic headgroups and the metal halide octahedra, etc., as discussed in detail in a variety of works.[1,45−47] In the radiative recombination process, electron−phonon coupling plays an important role, as it provides the necessary momentum and energy for the relaxation of the charge carriers to band edge states.[48] Furthermore, the deformation of the lattice induced by the electrical charges can enable the self-trapping of excitons.[33,49,50] From the complexity of Raman spectra of 2DLPs (see the example in Figure 1C), that feature a large variety of equally strong phonon bands, we can already guess that electron−phonon coupling models considering Fröhlich interaction[51,52] and only one (typically LO) phonon mode should fall short of an accurate description of their photophysics. This is even more the case because these phonon bands have significantly different properties in terms of symmetry and directionality, as we will discuss in this Account.

2.1. Impact of Architecture Anisotropy on the Emission Color

In our work published in *Advanced Materials* in 2019,[53] we observed the tunability of the emission of ensembles of $(DA)_2PbBr_4$ microcrystals by applying pressures in the low MPa range. This led to quenching of the low-energy emission band under such mild compression, resulting in blue light emission under pressure and white light when the pressure was released (Figure 2A,B). Structural changes induced by compression in the GPa range have been reported for lead iodide 2D perovskites,[54] that also had significant impact on the spectral emission properties. However, compressive stress in the range up to 10 MPa is not likely to result in significant lattice distortions,[55,56] and therefore, we attributed this emission color change to the reduced thickness of the 2DLP film that goes along with horizontal alignment of the microcrystal plates. Both effects should result in a reduction in the reabsorption within the film, which enhances the contribution of the blue band edge emission. This interpretation was supported by our density functional theory (DFT) calculations of the absorption bands in the in-plane and out-of-plane directions of the octahedron lattice (see Figure 2C,D). We further explored this concept by embedding $(BzA)_2PbBr_4$ microcrystals in a stretchable polydimethylsiloxane (PDMS) film that enabled mechanical switching of the emission intensity by stretch and release of the free-standing film,[57] as shown in Figure 2E. Also in this case the reabsorption was reduced in the stretched film, which led to higher emission intensity and spectral shifts of the emission peak.

2.2. Impact of Organic Cations on Emission Color and Phonon Bands

Figure 3 shows the emission spectra of various lead-bromide 2DLPs that differ in their organic cations. In our work in ref.,[43] we classified the cations according to their binding head groups in type-I, type-II and type-III ammoniums. Figure 3A-B shows that the emission color depends strongly on the ammonium type, allowing to tune from almost pure (blue) band edge emission to warm and cold white emission that is dominated by (self-) trapped excitons. Within the primary (type-I) ammonium 2DLPs, we investigated molecules with aliphatic chain and phenyl-ring backbones and found slight shifts in their band edge emission wavelength that could be mainly attributed to different dielectric confinements (Figure 3C). The intensity of the broad band emission associated with self-trapped excitons (STE) depended strongly on the type of headgroup, as evident in Figure 3B. Modeling of the accommodation of the headgroup in the voids of the octahedron lattice evidenced the conformation of the organic cations and the induced lattice distortions. The more bulky head groups led to increased STE emission, which was related to Jahn−Teller distortions.[59] For the evaluation of the electron−phonon coupling strength related to such broad emission, a model for the line width broadening of the emission of color centers[60] has been successfully applied to the thermal emission behavior of double perovskites.[31,61] However, when we applied this analysis to the 2DLPs with type-II and type-III ammonium molecules, we did not obtain a satisfactory fitting of the emission line width, which we attributed to the large number of dominant phonon bands that we observed in these materials.[2]

Evidencing the complex vibrational properties of the 2DLPs, our low-frequency Raman spectroscopy studies (Figure 3D) revealed very different phonon bands for $(PEA)_2PbBr_4$ (phenyl-ring molecule with more rigid $\pi-\pi$ stacking in the van der Waals gap) than for $(BA)_2PbBr_4$ that has a tail-to-tail arrangement of the aliphatic chains. We assigned these different sets of Raman peaks to phonon bands associated with distinct vibrational motions (see Table 1),[1] in agreement with other works.[45] Interestingly, we found more phonon modes in the $(PEA)_2PbBr_4$ bands (with respect to $(BA)_2PbBr_4$), which we tentatively assigned to mode splitting due to vibrational coupling between the layers. In ref 2 we also explored the interpretation of coupled acoustic modes for the origin of the low-frequency Raman peaks by applying the Rytov model of backfolded superlattice modes;[62,63] however, we could only achieve reasonable agreement with our data by assuming elastic parameters for the organic−inorganic layers that were different from those of their bulk material components.

Table 1. Frequencies of the Vibrational Modes Discerned in the Raman Spectra for $(PEA)_2PbBr_4$ and $(BA)_2PbBr_4$ Flakes at T = 4K, Together with Their Symmetry and the Tentative Assignment of the Dominant Vibrational Motion[1]

	frequency (cm^{-1})			
band	$(PEA)_2PbBr_4$	$(BA)_2PbBr_4$	irreducible representation (D_{2h} symmetry)	vibrational motion
M1	26.8	21.8	B_{1g}, B_{3g}	octahedron rocking/twisting
M2	52.4	35.7	A_g	Pb−Br bond bending
	54.9			
	56.0	44.9		
	57.7	50.3		
	58.8			
M3	70.3	61.5	B_{2g}	Pb−Br bond bending and twisting; Br−Pb−Br scissoring in the octahedral plane
	72.0			
	75.0			
	78.5			
	80			
M4	95.1	83.6	A_g	out-of-plane Pb−Br bond stretching
	105.3	89.1		
M5	131.6	106.8	A_g	in/out-of-plane Pb−Br bond stretching
	140.7	132		

https://doi.org/10.1021/acs.accounts.4c00259
Acc. Chem. Res. 2024, 57, 2476−2489

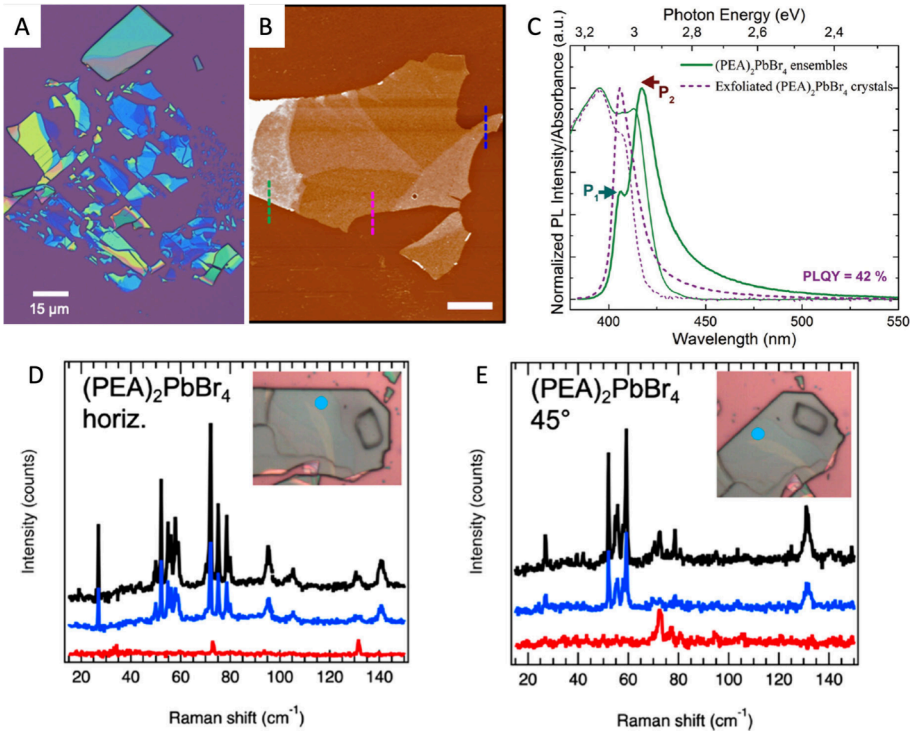

Figure 4. Exfoliation of single 2D perovskite flakes and the directional dependence of the optical and vibrational spectra. (A) Optical and (B) atomic force microscopy images of exfoliated flakes, where the height profiles along the green, pink, and blue dashed lines reveal thicknesses of 20, 14, and 10 nm, respectively. (C) PL spectra recorded from powders and exfoliated crystals. Reproduced from ref 58. CC BY-NC 3.0. (D, E) Raman spectra recorded from a single flake with horizontal (D) or diagonal (E) orientation with respect to the detection optics. The black, blue, and red colors refer to unpolarized, polarized, and depolarized configurations. The blue dots indicate the measurement spot. Reproduced from ref 1. Copyright 2020 American Chemical Society.

3. PHONON DIRECTIONALITY AND EMISSION POLARIZATION OF SINGLE MICROCRYSTALS

From our studies on ensembles (powders) of 2DLP microcrystals, we observed that the choice of the organic cation has a strong impact on both their optical and vibrational properties. However, such powder measurements are not adequate to explore the strong anisotropy of the 2DLP microcrystals since they average over many different orientations of the individual crystals. We therefore turned to investigate single microcrystals obtained by mechanical (Scotch tape) exfoliation (Figure 4A). Such exfoliation led in many cases to flakes with straight edges and well-defined angles at the corners that enabled us to explore the effect of the orientation of the octahedron lattice on the optical properties with micro-photoluminescence (micro-PL) and micro-Raman spectroscopy. Mechanical exfoliation leads to microcrystal flakes with thicknesses ranging from few nanometers up to several hundred nanometers, resulting different colors of the flakes in the optical microscopy image in Figure 4A caused by thin-film optical interference. The thinnest flakes that we measured were 8−10 nm in height (Figure 4B and ref 58), which, with interlayer spacing of ca. 1.5 nm, corresponds to approximately six monolayers of octahedron lattice planes. Interestingly, we observed that for materials from the same batch, the PL from powders had a double peak structure in the band edge emission, while from the exfoliated flakes we measured only a single peak that coincided with the higher-energy peak of the powders (Figure 4C).[58] Furthermore, the PL quantum yield from the exfoliated flakes (42%) was much higher than that of the powders (15%). We attributed this behavior to the different confinement in out-of-plane and in-plane directions (as discussed in Figure 2D), which in ensembles of differently oriented microcrystals favors reabsorption of the higher-energy light and re-emission from lower energy levels with lower transition rates. This interpretation was supported by the longer decay time of the low-energy emission peak[58] and by modeling of the absorption coefficients in the different directions.[64]

With our low-frequency Raman spectroscopy experiments,[1] we discovered that the phonon spectra measured from single-crystalline regions of lead bromide microcrystals depend strongly on the orientation of the microcrystal with respect to the polarization optics of the setup (Figure 4D,E). Comparing spectra recorded with parallel (horizontal) and diagonal configurations reveals that some phonon bands appear only at certain angles; thus, their intensity is highly directional (see, for example, the band around 50 cm^{-1} in Figure 4D,E that is absent in the spectra of the diagonal orientation). We investigated also flakes with different thicknesses and found that the profile of the Raman spectrum was not affected by the number of layers in the flake and that only the intensity scaled with the overall thickness. However, the band edge PL showed a slight dependence on the flake thickness, manifesting a red shift of a few nanometers with increasing number of layers from 15 to 75 (see Figure S4 in ref 1), which we tentatively assigned to self-absorption.

To delve deeper into the directionality of the different phonon bands, we extended our Raman setup to angle-resolved polarized Raman spectroscopy.[2,65] With this setup we recorded the angular dependence of the Raman signal in polarized (VV) and depolarized (HV) configurations, as illustrated in Figure 5A,B. Color maps of the Raman intensity

https://doi.org/10.1021/acs.accounts.4c00259
Acc. Chem. Res. 2024, 57, 2476−2489

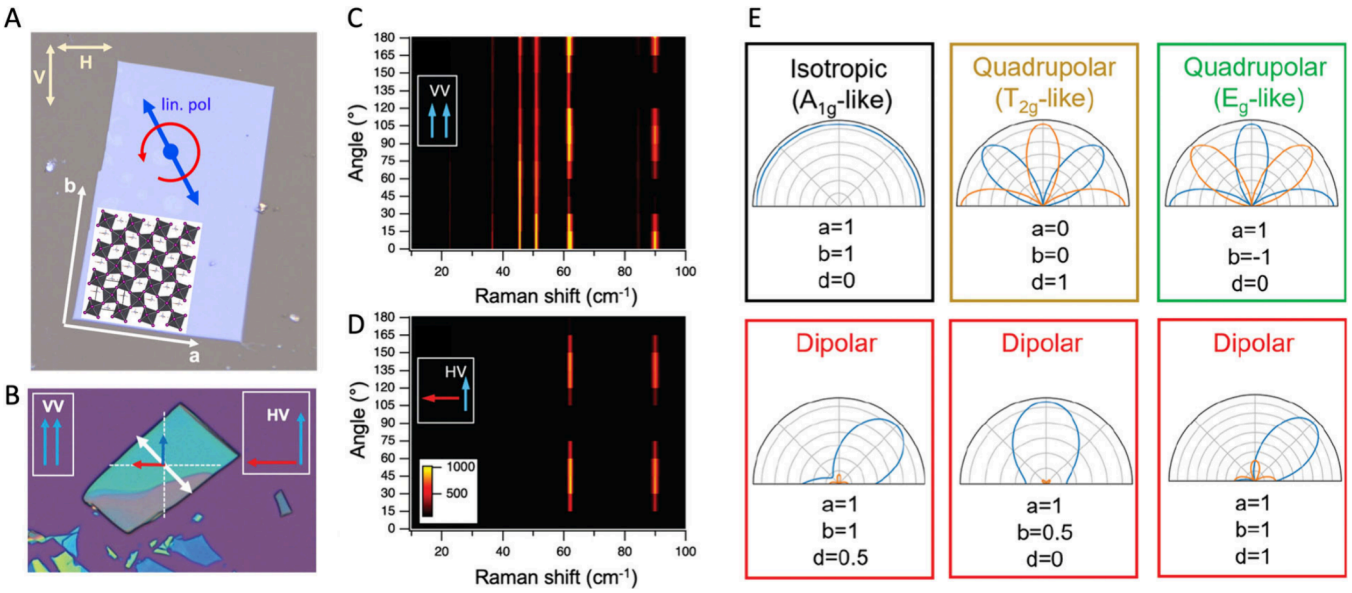

Figure 5. Angle-resolved polarized Raman spectroscopy on single flakes. (A, B) Illustration of the relative orientation of the perovskite octahedron lattice with respect to the polarizers in the excitation/detection paths (V, H) and of the rotation of the linear polarization with respect to the sample. Schemes are superimposed on an optical microscopy image of a single microcrystal. (C, D) Color map of angle-resolved Raman spectra recorded in polarized (VV) and depolarized (HV) configurations. Reproduced from ref 2. CC BY-NC 4.0. (E) Relation of the Raman tensor to the angular mode intensities, resulting in isotropic, bipolar, or quadrupolar modes. Reproduced with permission from ref 3. Copyright 2022 Wiley-VCH.

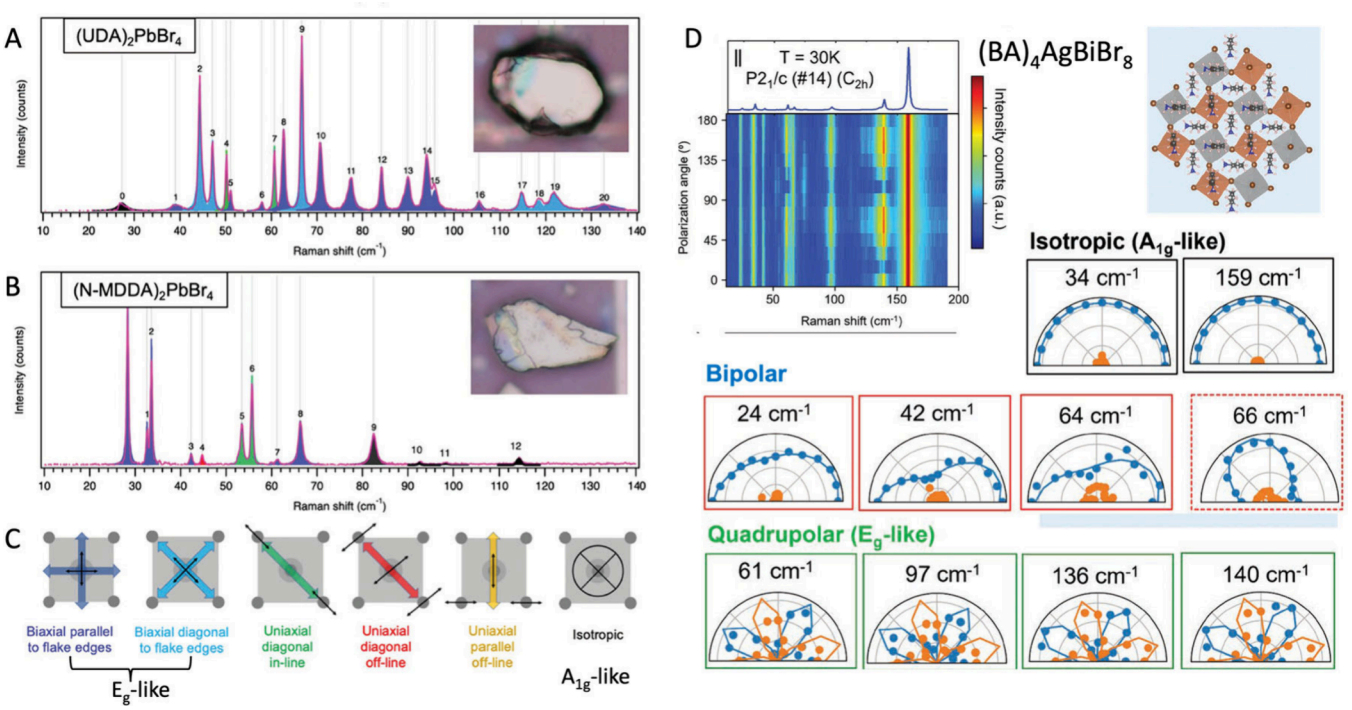

Figure 6. Assignment of the directional behavior of the phonon modes detected by Raman spectroscopy from single flakes. (A–C) Raman spectra recorded from lead bromide 2D perovskites at cryogenic temperature. The directional properties color-coded in (A) and (B) and illustrated in (C) were extracted from angular intensity mapping in polarized and depolarized configurations. Reproduced from ref 2. CC BY-NC 4.0. (D) Angle-resolved Raman data from 2D double perovskites and classification of the modes with respect to the symmetries of the Raman tensor. Reproduced with permission from ref 3. Copyright 2022 Wiley-VCH.

versus angle and frequency are displayed in Figure 5C,D (recorded from $(BA)_2PbBr_4$ at T = 5 K with below-band-gap excitation at 633 nm). Clearly, the different phonon modes show very diverse angular behavior, featuring one or two intensity maxima or almost constant intensity, in agreement with literature.[34] Note that the maxima of the same mode are shifted by 45° in HV with respect to VV, which indicates directionality along the two orthogonal axes that we associated with the major axes of the octahedron lattice. Such directional behavior can be rationalized and modeled by different

https://doi.org/10.1021/acs.accounts.4c00259
Acc. Chem. Res. 2024, 57, 2476–2489

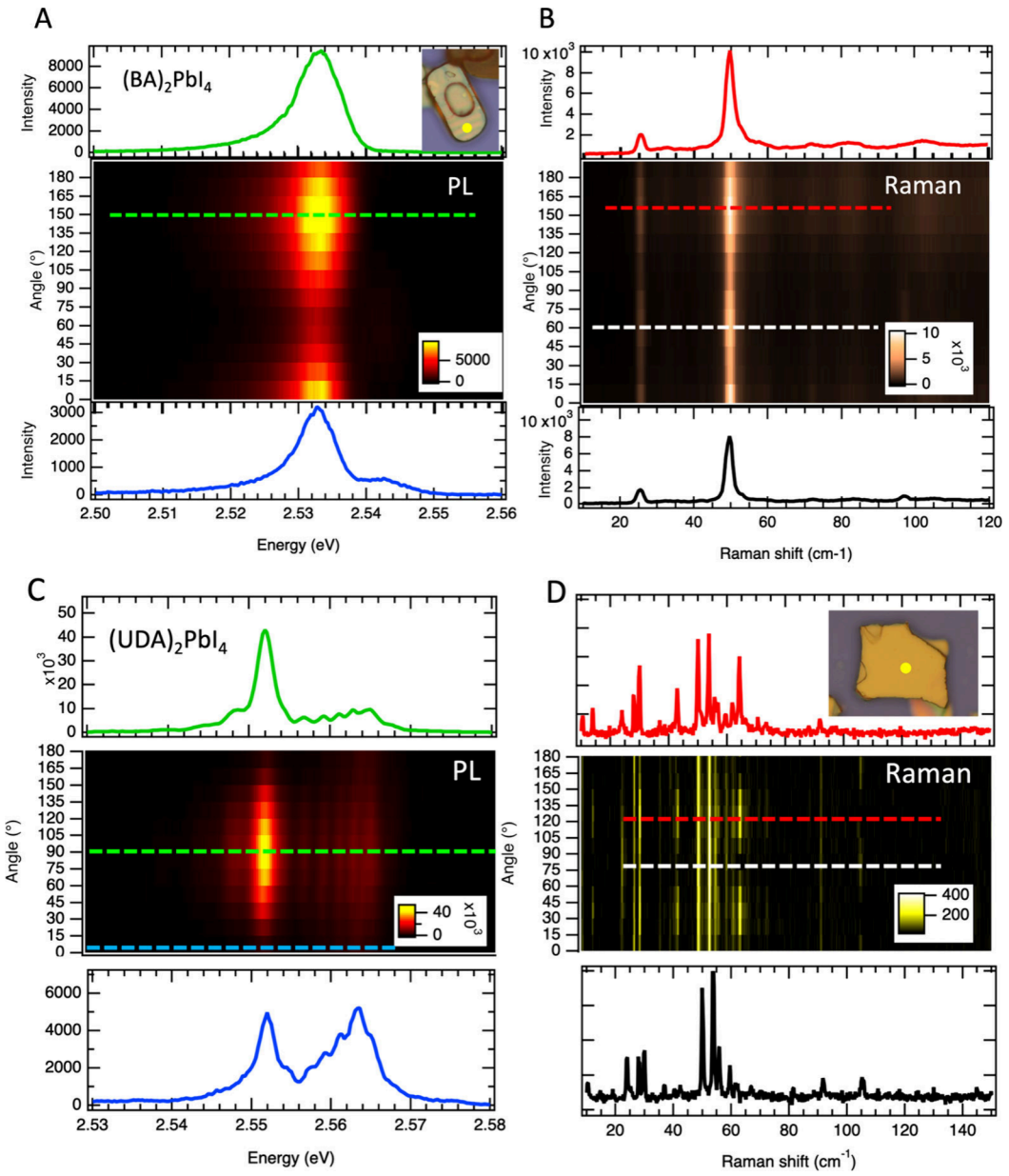

Figure 7. Correlation of PL and Raman spectra recorded from the same lead iodide microcrystal. Insets show optical microscopy images of the investigated flakes, and the yellow dots indicate the measurement spot. (A, C) Angle-resolved PL spectra from single exfoliated $(BA)_2PbI_4$ and $(UDA)_2PbI_4$ microcrystals. Spectra at the angles indicated by the green (blue) dashed lines are shown in the top (bottom) panels. (B, D) Angle dependence of the phonon bands measured by resonant (B) and nonresonant (D) Raman spectroscopy. The bottom (top) panels show spectra recorded at the angles indicated by the red (white) dashed lines. Adapted from ref 4.

symmetries of the Raman tensor, as shown by the polar plots in Figure 5E.

For nonresonant excitation, the Raman scattering intensity can be expressed by the Raman tensor as

$$I_R \propto \left| \overrightarrow{\mathbf{e}_s}^T \cdot \overleftrightarrow{\mathbf{R}} \cdot \overrightarrow{\mathbf{e}_i} \right|^2 \tag{1}$$

Here $\mathbf{e}_i$ and $\mathbf{e}_s$ are the vectors of the incident and scattered light: $\mathbf{e}_i = \mathbf{e}_s = (\cos\theta, \sin\theta, 0)$ for the VV configuration (where θ is the relative angle between the laser polarization vector and the crystallographic axis that was controlled by the $\lambda/2$ wave plate), while $\mathbf{e}_i = (\cos\theta, \sin\theta, 0)$ and $\mathbf{e}_s = (-\sin\theta, \cos\theta, 0)$ for the HV configuration. $\overleftrightarrow{R}$ is the Raman tensor with

$$\overleftrightarrow{\mathbf{R}} = \begin{pmatrix} a & d & \cdot \\ d & b & \cdot \\ \cdot & \cdot & \cdot \end{pmatrix} \tag{2}$$

where the coefficients related to the z direction have been replaced by dots since in our in-plane analysis they are not considered. Under VV polarization, the intensity of one phonon follows $I \propto |a\cos^2\theta + b\sin^2\theta + 2d\sin\theta\cos\theta|^2$, while under HV polarization it is $I \propto |(a-b)\sin^2\theta\cos^2\theta + d|^2$. Thus, it is possible to assign the phonon symmetries by comparing the experimental and calculated angular patterns, for example, the isotropic A_{1g}-like mode for $a = b = 1$ and $d = 0$ and the T_{2g}- and E_g-like symmetries for the quadrupolar modes.

https://doi.org/10.1021/acs.accounts.4c00259
Acc. Chem. Res. 2024, 57, 2476−2489

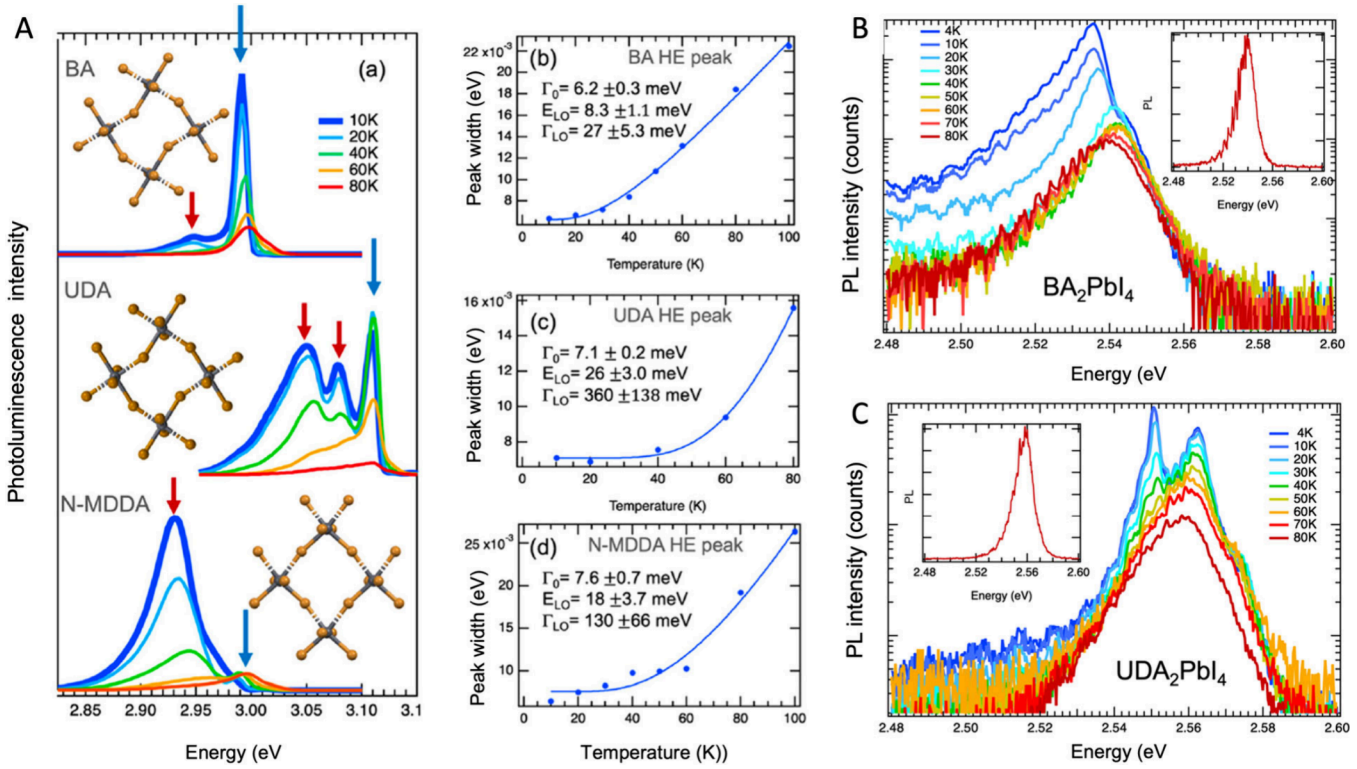

Figure 8. Temperature dependence of the band edge emission. (A) (a) PL recorded from 2D lead bromide microcrystal powders with BA, UDA, and N-MDDA as organic cations at cryogenic temperatures with laser excitation at 375 nm. (b–d) Fitting of the Gaussian line width broadening of the peak indicated by the blue arrow with eq 3. Reproduced from ref 35. CC BY-NC 3.0. (B, C) PL spectra recorded from single lead iodide microcrystals shown on a semilogarithmic scale. Adapted from ref 4.

We also obtained detailed insights into the directionality of the vibrational modes by a careful geometrical analysis of the angle-resolved Raman spectra in polarized (VV) and depolarized (HV) configurations, as specified in Figure 6A–C. We could identify modes along both major axes of the octahedron lattice (quadrupolar) that can stem from octahedron rocking or metal–halide bond stretching (dark blue), modes along only one direction (dipolar), with oscillations either along the same direction (green, bond stretching), perpendicular to it (red, bond bending), or both (yellow, bond scissoring), and isotropic modes that we assigned to out-of-plane oscillations. Interestingly, the UDA sample in Figure 6A manifests strong contributions of quadrupolar modes along directions diagonal to the other set of quadrupolar modes, which have a significant impact on the linear polarization of the emission, as we found out in our recent study that enabled us to record also angle-resolved polarized emission in addition to the Raman signal.[4] In general, we observed highly complex phonon spectra that contain a lot of low-frequency modes with different directionality from a large variety of 2DLPs comprising various organic cation types and bromide and iodide as halides.[2,4,43]

We extended our study to double perovskites, which represent a promising approach to replace the toxic Pb^{2+} metal cation, for example, by Ag^{+} and Bi^{3+}.[66] Such double perovskites can be fabricated as layered low-dimensional systems[67,68] and in the two-dimensional case have the $(Rm)_4AgBiBr_8$ structure (Rm is the organic cation) that features a checkerboard arrangement in the plane of the octahedron lattice (see Figure 6D). We investigated bulk $Cs_2AgBiBr_6$ crystals and the low-dimensional systems with two (2L) and one (1L) octahedron layers using BA as the organic cation.[3] Figure 6D shows a color plot of the angle-dependent polarized Raman spectra for the two-dimensional (1L) system, which demonstrates a similar behavior as their lead halide counterparts. The well-defined orientation of the octahedral lattice and support of DFT calculations allowed for a detailed microscopic and group theory assignment of the Raman modes. In this work we identified also soft Raman modes that were sensitive to phase transitions of the materials and could be used to distinguish first- from second-order transitions and determine the temperatures at which those phase transitions occurred.

Our work on two-dimensional double perovskites and lead iodide 2DLPs with different organic cations showed that the highly complex angular behavior of the vibrational bands is not restricted to the lead bromide system and should be a general consequence of the sophisticated anisotropic architecture of 2DLPs.

3.1. Combined Emission and Raman Spectroscopy on Single Microcrystals

Concerning the impact of electron–phonon coupling on the microcrystal emission, it would be very interesting to investigate the same microcrystal with both angle-resolved Raman and PL spectroscopy. Unfortunately, the optics of our cryogenic micro-PL (micro-Raman) setup are not UV-compatible, and therefore, excitation far above the band gap of the lead bromide 2DLPs was not possible at cryogenic temperatures. However, the exciton fine structure only emerges below ca. 100 K, as will be shown later. Therefore, we turned to lead iodide 2DLPs that emit in the green and where blue laser light can be used for the PL and Raman studies.[4] Our

https://doi.org/10.1021/acs.accounts.4c00259
Acc. Chem. Res. 2024, 57, 2476–2489

results for BA and UDA ammonium molecules as organic cations are displayed in Figure 7. Interestingly, although the difference of these molecules is only in their aliphatic chain length (4 carbons vs 11 carbons), they feature very different emission and vibrational properties in both their mode spectra and their angular dependence. For $(BA)_2PbI_4$ (Figure 7A), we observe two emission modes with orthogonal in-plane polarization (in agreement with ref 69), which goes along with dominant Raman bands around 25 and 50 cm^{-1} that under resonant (above-band-gap) excitation have their intensity maxima at nearly the same angles as the PL (Figure 7B). With nonresonant excitation, we can resolve a more detailed phonon spectrum, where also a few weaker side bands with their maxima shifted by 45° can be noted, for example in the range from 50 to 60 cm^{-1}.[4]

Turning to $(UDA)_2PbI_4$, we observe a very different behavior. Here all of the PL peaks have their intensity maximum at the same polarization angle (at 90° for this flake), and the intensity of the phonon modes under resonant excitation is almost independent of the polarization angle. Concerning the different PL peaks, we can distinguish a certain set of peaks that have different intensity increases with the angle; therefore, a signature of the in-plane polarization of the confined modes is present. With nonresonant Raman scattering (Figure 7C), we distinguish a very large number of phonon modes in the low-frequency regime that can be assigned similar to the lead bromide modes discussed above. The particular feature of the Raman bands of $(UDA)_2PbI_4$ is that a large number of modes with polarization at diagonal directions is present. These nonorthogonal modes can couple, and therefore, phonon modes with different directionality and energy can contribute to the electron−phonon coupling related to a specific emission peak. This mixing causes all emission peaks have their maximum at the same angle, which can be shifted with respect to the directions of the phonon modes.

4. TEMPERATURE DEPENDENCE OF EMISSION AND ELECTRON−PHONON COUPLING

The strong impact of the low-frequency phonons and electron−phonon coupling on the emission properties of the 2DLPs is also evident in the temperature dependence of the photoluminescence. The different sets of peaks that characterize the exciton fine structure emerge at temperatures below 100 K (Figure 8), thus in a range that corresponds to thermal energies below 10 meV (80 cm^{-1}), in which we observe the large number of low-frequency phonon bands. We investigated the temperature dependence of the emission of lead bromide 2DLPs with different organic cations[35] and observed different sets of emission peaks for the different materials that emerged below 100 K, as shown in Figure 8A. For the evaluation of the electron−phonon coupling, we focused on the high-energy peak in the band edge emission that is the most dominant in this temperature range and analyzed its thermal broadening by Gaussian line width fitting.

The thermal broadening of the PL of polar semiconductors can be described by[28]

$$\Gamma(T) = \Gamma_0 + \Gamma_{LO}/[\exp(E_{LO}/k_BT) - 1] \quad (3)$$

if we neglect coupling to acoustic phonons[70] and the scattering due to impurities. Here Γ_0 is the PL line width at zero temperature, Γ_{LO} is the coefficient for the exciton−optical phonon interaction, E_{LO} is the average energy of the longitudinal optical (LO) phonon modes involved in the coupling, and k_B is the Boltzmann constant. As can be seen in Figure 8A(b−d), the fitting works quite well for the BA system, which has relatively few phonon modes in the low-frequency range, and yields an LO phonon energy of 8.3 meV that matches well the M3 band discussed in Figure 3. For the UDA and N-MDDA systems, the fitting is much less accurate (precise fitting was also made difficult by strong changes in the spectral shape with temperature), and we obtained high phonon energy values of 26 and 18 meV that did not correspond to any dominant Raman bands in our experiments. Furthermore, we obtained a very high value of 360 meV for the electron−phonon coupling, which goes along with the very large number of low-frequency phonon modes that we observed for the UDA system. We therefore hypothesized that the combination of different phonon modes and two-phonon scattering (as reported for bilayer WSe_2,[71]) could be the reason for obtaining such high phonon energy values in the fitting. However, phonon mode intensities can strongly change with resonance conditions,[29,72] which motivated the investigation of single 2DLP flakes under resonant and nonresonant conditions in combination with the measurement of their angular emission properties[4] that we already discussed in Figure 7. In these experiments, we did not observe the appearance of strong phonon bands at high energies (in the 20−40 meV range), but we found evidence of mixing of phonon bands with different directionalities as discussed above, which supports the interpretation of the involvement of two-phonon scattering events in the thermal emission line width broadening. The temperature-dependent emission spectra of $(BA)_2PbI_4$ and $(UDA)_2PbI_4$ in the range below 100 K are shown in Figure 8B,C. Gaussian fitting to extract the line width is hindered by the change in spectral shape, since for $(BA)_2PbI_4$ a pronounced low-energy tail emerges with decreasing temperature, while for $(UDA)_2PbI_4$ the emission band splits into a high- and low-energy doublet. This behavior evidences the thermal (phonon) coupling of the different exciton levels at the band edge, in which the highest-energy peak, related to the out-of-plane confinement, has the strongest oscillator strength and therefore dominates the emission.

5. SUMMARY AND OUTLOOK

The emission and Raman spectroscopy studies showed that two-dimensional hybrid organic−inorganic metal halide crystals are a very particular system in which the properties of soft organic phases and rigid inorganic lattices are strongly intertwined. The inorganic (semiconducting) metal halide octahedron lattice is the origin of the electronic-level structure, but the organic phases alter the optoelectronic properties due to lattice distortions, different confinement conditions, and diverse vibrational coupling. This on one hand allows for a very large freedom to engineer materials with diverse properties but on the other hand also complicates the modeling and prediction of their optoelectronic behavior. Furthermore, due to their layered architecture, these materials feature strong anisotropies in their optical, electrical, and elastic properties, and our single-microcrystal studies evidenced that in addition to the obvious out-of-plane anisotropies there are also subtle in-plane effects that affect the phonon bands, electron−phonon coupling, and thereby the emission polarization. Such effects of the architecture anisotropy become particularly evident for single-microcrystal studies. For example, the reabsorption of the emitted light is favored in ensembles of differently oriented

https://doi.org/10.1021/acs.accounts.4c00259
Acc. Chem. Res. 2024, 57, 2476−2489

microcrystals (due to the band gap differences along the different crystal directions), while single microcrystals and thin films of aligned crystals show a much higher emission quantum yield. Furthermore, the phonon spectra of single microcrystals depend strongly on the relative orientation of the microcrystal lattice and the polarization of the incident light because many phonon bands feature a strong directionality. Also, the emission manifests polarization anisotropies that in some cases go along with the spatial confinement, leading to level splitting in the exciton fine structure and therefore polarization along the corresponding *x*, *y*, and *z* spatial directions.[69] However, in 2DLPs that feature dominant phonon bands in nonorthogonal directions, in particular along major crystal axes and their diagonals, multiphonon coupling in the optical relaxation process can mix the polarization dependence and alter the emission polarization. The involvement of several phonon modes in the emission process renders commonly used models for electron−phonon coupling (based on coupling to a single LO phonon mode) inaccurate. On the other hand, a deeper understanding of the electron−phonon coupling in 2DLPs can open avenues to tailor their emission properties by acting on the type of organic cation. We saw in the examples of the BA and UDA systems that only a small change in the length of the aliphatic chain can significantly change the emission spectrum, polarization, and quantum yield. Such tunability can be highly interesting toward optical devices based on single microcrystals. In this respect, the recent trends in using automated synthesis methods together with artificial intelligence and machine learning to design and characterize such complex materials open promising avenues to gain control over their structural and optoelectronic properties.[73−76] Due to their high dielectric permittivity in the visible,[77−79] 2DLP microcrystals can act as photonic cavities[80] and, for example, give rise to exciton−polaritons.[81] Here tuning the emission polarization will be highly interesting to enhance the performance and functionality of such single-crystal photonic structures. Therefore, gaining knowledge of how the vibrational properties and exciton−phonon coupling determine the emission properties of 2DLPs will be highly versatile for optical applications of these materials, and we hope that this Account could give a useful contribution in this respect.

AUTHOR INFORMATION

Corresponding Author

Roman Krahne − *Optoelectronics, Istituto Italiano di Tecnologia (IIT), 16163 Genoa, Italy;* orcid.org/0000-0003-0066-7019; Email: roman.krahne@iit.it

Authors

Miao-Ling Lin − *State Key Laboratory of Superlattices and Microstructures, Institute of Semiconductors, Chinese Academy of Sciences, Beijing 100083, China; Center of Materials Science and Optoelectronics Engineering and CAS Center of Excellence in Topological Quantum Computation, University of Chinese Academy of Sciences, Beijing 100049, China;* orcid.org/0000-0001-5838-8237

Ping-Heng Tan − *State Key Laboratory of Superlattices and Microstructures, Institute of Semiconductors, Chinese Academy of Sciences, Beijing 100083, China; Center of Materials Science and Optoelectronics Engineering and CAS Center of Excellence in Topological Quantum Computation, University of Chinese Academy of Sciences, Beijing 100049, China;* orcid.org/0000-0001-6575-1516

Complete contact information is available at: https://pubs.acs.org/10.1021/acs.accounts.4c00259

Author Contributions

The manuscript was written through contributions of all authors. All of the authors approved the final version of the manuscript. CRediT: **Roman Krahne** conceptualization, formal analysis, funding acquisition, investigation, methodology, supervision, visualization, writing-original draft, writing-review & editing; **Miao-Ling Lin** data curation, formal analysis, funding acquisition, investigation, methodology, writing-review & editing; **Ping-Heng Tan** conceptualization, funding acquisition, methodology, resources, supervision, writing-review & editing.

Notes

The authors declare no competing financial interest.

Biographies

Roman Krahne is Senior Researcher at the Italian Institute of Technology and Leader of the Optoelectronics Research Line. He received his Ph.D. in physics from the University of Hamburg, worked as a postdoctoral fellow at the Weizmann Institute of Science, and was appointed Honorary Professor at the Institute of Semiconductors, Chinese Academy of Sciences. His research is focused on the photophysics and optoelectronic properties of nanostructured systems such as colloidal nanocrystals, two-dimensional materials, and photonic metamaterials.

Miao-Ling Lin is Professor at the Institute of Semiconductors, Chinese Academy of Sciences. She graduated from the School of Physics of Nankai University in 2014 and obtained her Ph.D. from the University of Chinese Academy of Sciences in 2019. Her current research interest focuses on phonon physics and optical properties of low-dimensional semiconductors.

Ping-Heng Tan is Professor at the Institute of Semiconductors, Chinese Academy of Sciences. He obtained his B.S. in Physics from Peking University in 1996 and his Ph.D. from the Institute of Semiconductors, Chinese Academy of Sciences in 2001. He worked at the Walter Schottky Institut, Technische Universität München as a Postdoctoral Research Associate in 2001−2003 and was a KC-Wong Royal Society Fellow at Cambridge University in 2006−2007. His current research is on 2D layered materials, nanocarbon materials, topological insulators, and novel low-dimensional semiconductor optoelectronic materials.

ACKNOWLEDGMENTS

R.K. acknowledges funding by the European Union under Project 101131111 − DELIGHT. P.-H.T. and M.-L.L. acknowledge support from the National Natural Science Foundation of China (Grants 12322401 and 12127807), the Beijing Nova Program (Grant 20230484301), and the Youth Innovation Promotion Association, Chinese Academy of Sciences (2023125).

REFERENCES

(1) Dhanabalan, B.; Leng, Y.-C.; Biffi, G.; Lin, M.-L.; Tan, P.-H.; Infante, I.; Manna, L.; Arciniegas, M. P.; Krahne, R. Directional Anisotropy of the Vibrational Modes in 2D-Layered Perovskites. *ACS Nano* **2020**, *14*, 4689−4697.

(2) Lin, M.-L.; Dhanabalan, B.; Biffi, G.; Leng, Y.-C.; Kutkan, S.; Arciniegas, M. P.; Tan, P.-H.; Krahne, R. Correlating Symmetries of Low-Frequency Vibrations and Self-Trapped Excitons in Layered Perovskites for Light Emission with Different Colors. *Small* **2022**, *18*, No. 2106759.
(3) Martín-García, B.; Spirito, D.; Lin, M.-L.; Leng, Y.-C.; Artyukhin, S.; Tan, P.-H.; Krahne, R. Low-Frequency Phonon Modes in Layered Silver-Bismuth Double Perovskites: Symmetry, Polarity, and Relation to Phase Transitions. *Adv. Opt. Mater.* **2022**, *10*, No. 2270056.
(4) Krahne, R.; Schleusener, A.; Faraji, M.; Li, L.-H.; Lin, M.-L.; Tan, P.-H. Phonon Directionality Impacts Electron-Phonon Coupling and Polarization of the Band-Edge Emission in Two-Dimensional Metal Halide Perovskites. *Nano Lett.*, DOI: 10.1021/acs.nanolett.4c03543.
(5) Mir, S. H.; Nagahara, L. A.; Thundat, T.; Mokarian-Tabari, P.; Furukawa, H.; Khosla, A. Review—Organic-Inorganic Hybrid Functional Materials: An Integrated Platform for Applied Technologies. *J. Electrochem. Soc.* **2018**, *165*, B3137.
(6) Wintzheimer, S.; Granath, T.; Oppmann, M.; Kister, T.; Thai, T.; Kraus, T.; Vogel, N.; Mandel, K. Supraparticles: Functionality from Uniform Structural Motifs. *ACS Nano* **2018**, *12*, 5093−5120.
(7) Ni, B.; Gonzalez-Rubio, G.; Cölfen, H. Self-Assembly of Colloidal Nanocrystals into 3D Binary Mesocrystals. *Acc. Chem. Res.* **2022**, *55*, 1599−1608.
(8) Marino, E.; LaCour, R. A.; Moore, T. C.; van Dongen, S. W.; Keller, A. W.; An, D.; Yang, S.; Rosen, D. J.; Gouget, G.; Tsai, E. H. R.; Kagan, C. R.; Kodger, T. E.; Glotzer, S. C.; Murray, C. B. Crystallization of Binary Nanocrystal Superlattices and the Relevance of Short-Range Attraction. *Nat. Synth.* **2024**, *3*, 111−122.
(9) Zhao, Q.; Hazarika, A.; Chen, X.; Harvey, S. P.; Larson, B. W.; Teeter, G. R.; Liu, J.; Song, T.; Xiao, C.; Shaw, L.; Zhang, M.; Li, G.; Beard, M. C.; Luther, J. M. High Efficiency Perovskite Quantum Dot Solar Cells with Charge Separating Heterostructure. *Nat. Commun.* **2019**, *10*, 2842.
(10) Stranks, S. D.; Snaith, H. J. Metal-Halide Perovskites for Photovoltaic and Light-Emitting Devices. *Nat. Nanotechnol.* **2015**, *10*, 391−402.
(11) Brenner, T. M.; Egger, D. A.; Kronik, L.; Hodes, G.; Cahen, D. Hybrid Organic—Inorganic Perovskites: Low-Cost Semiconductors with Intriguing Charge-Transport Properties. *Nat. Rev. Mater.* **2016**, *1*, 15007.
(12) Zhao, Y.; Zhu, K. Organic−Inorganic Hybrid Lead Halide Perovskites for Optoelectronic and Electronic Applications. *Chem. Soc. Rev.* **2016**, *45*, 655−689.
(13) Seok, S. I.; Grätzel, M.; Park, N.-G. Methodologies toward Highly Efficient Perovskite Solar Cells. *Small* **2018**, *14*, No. 1704177.
(14) Dong, H.; Ran, C.; Gao, W.; Li, M.; Xia, Y.; Huang, W. Metal Halide Perovskite for Next-Generation Optoelectronics: Progresses and Prospects. *eLight* **2023**, *3*, 3.
(15) Mao, L.; Stoumpos, C. C.; Kanatzidis, M. G. Two-Dimensional Hybrid Halide Perovskites: Principles and Promises. *J. Am. Chem. Soc.* **2019**, *141*, 1171−1190.
(16) Zhang, F.; Lu, H.; Tong, J.; Berry, J. J.; Beard, M. C.; Zhu, K. Advances in Two-Dimensional Organic−Inorganic Hybrid Perovskites. *Energy Environ. Sci.* **2020**, *13*, 1154−1186.
(17) Lin, H.; Zhou, C.; Tian, Y.; Siegrist, T.; Ma, B. Low-Dimensional Organometal Halide Perovskites. *ACS Energy Lett.* **2018**, *3*, 54−62.
(18) Mauck, C. M.; Tisdale, W. A. Excitons in 2D Organic−Inorganic Halide Perovskites. *Trends Chem.* **2019**, *1*, 380−393.
(19) Yuan, M.; Quan, L. N.; Comin, R.; Walters, G.; Sabatini, R.; Voznyy, O.; Hoogland, S.; Zhao, Y.; Beauregard, E. M.; Kanjanaboos, P.; Lu, Z.; Kim, D. H.; Sargent, E. H. Perovskite Energy Funnels for Efficient Light-Emitting Diodes. *Nat. Nanotechn.* **2016**, *11*, 872−877.
(20) Quintero-Bermudez, R.; Gold-Parker, A.; Proppe, A. H.; Munir, R.; Yang, Z.; Kelley, S. O.; Amassian, A.; Toney, M. F.; Sargent, E. H. Compositional and Orientational Control in Metal Halide Perovskites of Reduced Dimensionality. *Nat. Mater.* **2018**, *17*, 900−907.
(21) Stoumpos, C. C.; Cao, D. H.; Clark, D. J.; Young, J.; Rondinelli, J. M.; Jang, J. I.; Hupp, J. T.; Kanatzidis, M. G. Ruddlesden−Popper Hybrid Lead Iodide Perovskite 2D Homologous Semiconductors. *Chem. Mater.* **2016**, *28*, 2852−2867.
(22) Li, X.; Hoffman, J. M.; Kanatzidis, M. G. The 2D Halide Perovskite Rulebook: How the Spacer Influences Everything from the Structure to Optoelectronic Device Efficiency. *Chem. Rev.* **2021**, *121*, 2230−2291.
(23) Gong, Y.; Yue, S.; Liang, Y.; Du, W.; Bian, T.; Jiang, C.; Bao, X.; Zhang, S.; Long, M.; Zhou, G.; Yin, J.; Deng, S.; Zhang, Q.; Wu, B.; Liu, X. Boosting Exciton Mobility Approaching Mott-Ioffe-Regel Limit in Ruddlesden−Popper Perovskites by Anchoring the Organic Cation. *Nat. Commun.* **2024**, *15*, 1893.
(24) Wu, B.; Wang, A.; Fu, J.; Zhang, Y.; Yang, C.; Gong, Y.; Jiang, C.; Long, M.; Zhou, G.; Yue, S.; Ma, W.; Liu, X. Uncovering the Mechanisms of Efficient Upconversion in Two-Dimensional Perovskites with Anti-Stokes Shift up to 220 meV. *Sci. Adv.* **2023**, *9*, eadi9347.
(25) Li, J.; Wang, J.; Zhang, Y.; Wang, H.; Lin, G.; Xiong, X.; Zhou, W.; Luo, H.; Li, D. Fabrication of Single Phase 2D Homologous Perovskite Microplates by Mechanical Exfoliation. *2D Mater.* **2018**, *5*, No. 021001.
(26) Mante, P.-A.; Stoumpos, C. C.; Kanatzidis, M. G.; Yartsev, A. Electron−Acoustic Phonon Coupling in Single Crystal $CH_3NH_3PbI_3$ Perovskites Revealed by Coherent Acoustic Phonons. *Nat. Commun.* **2017**, *8*, No. 14398.
(27) Cho, Y.; Berkelbach, T. C. Optical Properties of Layered Hybrid Organic−Inorganic Halide Perovskites: A Tight-Binding Gw-Bse Study. *J. Phys. Chem. Lett.* **2019**, *10*, 6189−6196.
(28) Wright, A. D.; Verdi, C.; Milot, R. L.; Eperon, G. E.; Pérez-Osorio, M. A.; Snaith, H. J.; Giustino, F.; Johnston, M. B.; Herz, L. M. Electron-Phonon Coupling in Hybrid Lead Halide Perovskites. *Nat. Commun.* **2016**, *7*, 11755.
(29) Mauck, C. M.; France-Lanord, A.; Hernandez Oendra, A. C.; Dahod, N. S.; Grossman, J. C.; Tisdale, W. A. Inorganic Cage Motion Dominates Excited-State Dynamics in 2D-Layered Perovskites $(C_xH_{2x+1}NH_3)_2PbI_4$ (x = 4−9). *J. Phys. Chem. C* **2019**, *123*, 27904−27916.
(30) Iaru, C. M.; Geuchies, J. J.; Koenraad, P. M.; Vanmaekelbergh, D.; Silov, A. Y. Strong Carrier−Phonon Coupling in Lead Halide Perovskite Nanocrystals. *ACS Nano* **2017**, *11*, 11024−11030.
(31) Luo, J.; Wang, X.; Li, S.; Liu, J.; Guo, Y.; Niu, G.; Yao, L.; Fu, Y.; Gao, L.; Dong, Q.; Zhao, C.; Leng, M.; Ma, F.; Liang, W.; Wang, L.; Jin, S.; Han, J.; Zhang, L.; Etheridge, J.; Wang, J.; Yan, Y.; Sargent, E. H.; Tang, J. Efficient and Stable Emission of Warm-White Light from Lead-Free Halide Double Perovskites. *Nature* **2018**, *563*, 541−545.
(32) Li, S.; Luo, J.; Liu, J.; Tang, J. Self-Trapped Excitons in All-Inorganic Halide Perovskites: Fundamentals, Status, and Potential Applications. *J. Phys. Chem. Lett.* **2019**, *10*, 1999−2007.
(33) Ni, L.; Huynh, U.; Cheminal, A.; Thomas, T. H.; Shivanna, R.; Hinrichsen, T. F.; Ahmad, S.; Sadhanala, A.; Rao, A. Real-Time Observation of Exciton−Phonon Coupling Dynamics in Self-Assembled Hybrid Perovskite Quantum Wells. *ACS Nano* **2017**, *11*, 10834−10843.
(34) Menahem, M.; Dai, Z.; Aharon, S.; Sharma, R.; Asher, M.; Diskin-Posner, Y.; Korobko, R.; Rappe, A. M.; Yaffe, O. Strongly Anharmonic Octahedral Tilting in Two-Dimensional Hybrid Halide Perovskites. *ACS Nano* **2021**, *15*, 10153−10162.
(35) Kutkan, S.; Dhanabalan, B.; Lin, M.-L.; Tan, P.-H.; Schleusener, A.; Arciniegas, M. P.; Krahne, R. Impact of the Organic Cation on the Band-Edge Emission of Two-Dimensional Lead−Bromide Perovskites. *Nanoscale* **2023**, *15*, 12880−12888.
(36) Posmyk, K.; Dyksik, M.; Surrente, A.; Maude, D. K.; Zawadzka, N.; Babiński, A.; Molas, M. R.; Paritmongkol, W.; Mączka, M.; Tisdale, W. A.; Plochocka, P.; Baranowski, M. Exciton Fine Structure in 2D Perovskites: The Out-of-Plane Excitonic State. *Adv. Opt. Mater.* **2024**, *12*, No. 2300877.

(37) Posmyk, K.; Zawadzka, N.; Dyksik, M.; Surrente, A.; Maude, D. K.; Kazimierczuk, T.; Babiński, A.; Molas, M. R.; Paritmongkol, W.; Mączka, M.; Tisdale, W. A.; Płochocka, P.; Baranowski, M. Quantification of Exciton Fine Structure Splitting in a Two-Dimensional Perovskite Compound. *J. Phys. Chem. Lett.* **2022**, *13*, 4463−4469.
(38) Steger, M.; Janke, S. M.; Sercel, P. C.; Larson, B. W.; Lu, H.; Qin, X.; Yu, V. W.-z.; Blum, V.; Blackburn, J. L. On the Optical Anisotropy in 2D Metal-Halide Perovskites. *Nanoscale* **2022**, *14*, 752−765.
(39) Quarti, C.; Giorgi, G.; Katan, C.; Even, J.; Palummo, M. Exciton Ground State Fine Structure and Excited States Landscape in Layered Halide Perovskites from Combined BSe Simulations and Symmetry Analysis. *Adv. Opt. Mater.* **2024**, *12*, No. 2202801.
(40) Katan, C.; Mercier, N.; Even, J. Quantum and Dielectric Confinement Effects in Lower-Dimensional Hybrid Perovskite Semiconductors. *Chem. Rev.* **2019**, *119*, 3140−3192.
(41) Smith, M. D.; Karunadasa, H. I. White-Light Emission from Layered Halide Perovskites. *Acc. Chem. Res.* **2018**, *51*, 619−627.
(42) Smith, M. D.; Jaffe, A.; Dohner, E. R.; Lindenberg, A. M.; Karunadasa, H. I. Structural Origins of Broadband Emission from Layered Pb−Br Hybrid Perovskites. *Chem. Sci.* **2017**, *8*, 4497−4504.
(43) Dhanabalan, B.; Biffi, G.; Moliterni, A.; Olieric, V.; Giannini, C.; Saleh, G.; Ponet, L.; Prato, M.; Imran, M.; Manna, L.; Krahne, R.; Artyukhin, S.; Arciniegas, M. P. Engineering the Optical Emission and Robustness of Metal-Halide Layered Perovskites through Ligand Accommodation. *Adv. Mater.* **2021**, *33*, No. 2008004.
(44) Paritmongkol, W.; Powers, E. R.; Dahod, N. S.; Tisdale, W. A. Two Origins of Broadband Emission in Multilayered 2D Lead Iodide Perovskites. *J. Phys. Chem. Lett.* **2020**, *11*, 8565−8572.
(45) Thouin, F.; Valverde-Chávez, D. A.; Quarti, C.; Cortecchia, D.; Bargigia, I.; Beljonne, D.; Petrozza, A.; Silva, C.; Srimath Kandada, A. R. Phonon Coherences Reveal the Polaronic Character of Excitons in Two-Dimensional Lead Halide Perovskites. *Nat. Mater.* **2019**, *18*, 349−356.
(46) Straus, D. B.; Kagan, C. R. Electrons, Excitons, and Phonons in Two-Dimensional Hybrid Perovskites: Connecting Structural, Optical, and Electronic Properties. *J. Phys. Chem. Lett.* **2018**, *9*, 1434−1447.
(47) Straus, D. B.; Hurtado Parra, S.; Iotov, N.; Gebhardt, J.; Rappe, A. M.; Subotnik, J. E.; Kikkawa, J. M.; Kagan, C. R. Direct Observation of Electron−Phonon Coupling and Slow Vibrational Relaxation in Organic−Inorganic Hybrid Perovskites. *J. Am. Chem. Soc.* **2016**, *138*, 13798−13801.
(48) Straus, D. B.; Kagan, C. R. Photophysics of Two-Dimensional Semiconducting Organic−Inorganic Metal-Halide Perovskites. *Annu. Rev. Phys. Chem.* **2022**, *73*, 403−428.
(49) Srimath Kandada, A. R.; Silva, C. Exciton Polarons in Two-Dimensional Hybrid Metal-Halide Perovskites. *J. Phys. Chem. Lett.* **2020**, *11*, 3173−3184.
(50) Thouin, F.; Srimath Kandada, A. R.; Valverde-Chávez, D. A.; Cortecchia, D.; Bargigia, I.; Petrozza, A.; Yang, X.; Bittner, E. R.; Silva, C. Electron−Phonon Couplings Inherent in Polarons Drive Exciton Dynamics in Two-Dimensional Metal-Halide Perovskites. *Chem. Mater.* **2019**, *31*, 7085−7091.
(51) Iaru, C. M.; Brodu, A.; van Hoof, N. J. J.; ter Huurne, S. E. T.; Buhot, J.; Montanarella, F.; Buhbut, S.; Christianen, P. C. M.; Vanmaekelbergh, D.; de Mello Donega, C.; Rivas, J. G.; Koenraad, P. M.; Silov, A. Y. Fröhlich Interaction Dominated by a Single Phonon Mode in $CsPbBr_3$. *Nat. Commun.* **2021**, *12*, 5844.
(52) Sio, W. H.; Giustino, F. Unified Ab Initio Description of Fröhlich Electron-Phonon Interactions in Two-Dimensional and Three-Dimensional Materials. *Phys. Rev. B* **2022**, *105*, No. 115414.
(53) Castelli, A.; Biffi, G.; Ceseracciu, L.; Spirito, D.; Prato, M.; Altamura, D.; Giannini, C.; Artyukhin, S.; Krahne, R.; Manna, L.; Arciniegas, M. P. Revealing Photoluminescence Modulation from Layered Halide Perovskite Microcrystals Upon Cyclic Compression. *Adv. Mater.* **2019**, *31*, No. 1805608.
(54) Yin, T.; Liu, B.; Yan, J.; Fang, Y.; Chen, M.; Chong, W. K.; Jiang, S.; Kuo, J.-L.; Fang, J.; Liang, P.; Wei, S.; Loh, K. P.; Sum, T. C.; White, T. J.; Shen, Z. X. Pressure-Engineered Structural and Optical Properties of Two-Dimensional $(C_4H_9NH_3)_2PbI_4$ Perovskite Exfoliated nm-Thin Flakes. *J. Am. Chem. Soc.* **2019**, *141*, 1235−1241.
(55) Jaffe, A.; Lin, Y.; Karunadasa, H. I. Halide Perovskites under Pressure: Accessing New Properties through Lattice Compression. *ACS Energy Lett.* **2017**, *2*, 1549−1555.
(56) Yin, T.; Fang, Y.; Chong, W. K.; Ming, K. T.; Jiang, S.; Li, X.; Kuo, J.-L.; Fang, J.; Sum, T. C.; White, T. J.; Yan, J.; Shen, Z. X. High-Pressure-Induced Comminution and Recrystallization of $CH_3NH_3PbBr_3$ Nanocrystals as Large Thin Nanoplates. *Adv. Mater.* **2018**, *30*, No. 1705017.
(57) Dhanabalan, B.; Castelli, A.; Ceseracciu, L.; Spirito, D.; Di Stasio, F.; Manna, L.; Krahne, R.; Arciniegas, M. P. Mechanical Switching of Orientation-Related Photoluminescence in Deep-Blue 2D Layered Perovskite Ensembles. *Nanoscale* **2021**, *13*, 3948−3956.
(58) Dhanabalan, B.; Castelli, A.; Palei, M.; Spirito, D.; Manna, L.; Krahne, R.; Arciniegas, M. Simple Fabrication of Layered Halide Perovskite Platelets and Enhanced Photoluminescence from Mechanically Exfoliated Flakes. *Nanoscale* **2019**, *11*, 8334−8342.
(59) Wang, X.; Meng, W.; Liao, W.; Wang, J.; Xiong, R.-G.; Yan, Y. Atomistic Mechanism of Broadband Emission in Metal Halide Perovskites. *J. Phys. Chem. Lett.* **2019**, *10*, 501−506.
(60) Stadler, W.; Hofmann, D. M.; Alt, H. C.; Muschik, T.; Meyer, B. K.; Weigel, E.; Müller-Vogt, G.; Salk, M.; Rupp, E.; Benz, K. W. Optical Investigations of Defects in $Cd_{(1-x)}Zn_xTe$. *Phys. Rev. B* **1995**, *51*, 10619−10630.
(61) McCall, K. M.; Stoumpos, C. C.; Kostina, S. S.; Kanatzidis, M. G.; Wessels, B. W. Strong Electron−Phonon Coupling and Self-Trapped Excitons in the Defect Halide Perovskites $A_3M_2I_9$ (A = Cs, Rb; M = Bi, Sb). *Chem. Mater.* **2017**, *29*, 4129−4145.
(62) Rytov, S. M. Acoustical Properties of a Thinly Laminated Medium. *Sov. Phys.—Acoust.* **1956**, *2*, 68−80.
(63) Dahod, N. S.; France-Lanord, A.; Paritmongkol, W.; Grossman, J. C.; Tisdale, W. A. Low-Frequency Raman Spectrum of 2D Layered Perovskites: Local Atomistic Motion or Superlattice Modes? *J. Chem. Phys.* **2020**, *153*, No. 044710.
(64) Castelli, A.; Biffi, G.; Ceseracciu, L.; Spirito, D.; Prato, M.; Altamura, D.; Giannini, C.; Artyukhin, S.; Krahne, R.; Manna, L.; Arciniegas, M. P. Revealing Photoluminescence Modulation from Layered Halide Perovskite Microcrystals Upon Cyclic Compression. *Adv. Mater.* **2019**, *30*, No. 1805608.
(65) Liu, X.-L.; Zhang, X.; Lin, M.-L.; Tan, P.-H. Different Angle-Resolved Polarization Configurations of Raman Spectroscopy: A Case on the Basal and Edge Plane of Two-Dimensional Materials. *Chin. Phys. B* **2017**, *26*, No. 067802.
(66) Slavney, A. H.; Hu, T.; Lindenberg, A. M.; Karunadasa, H. I. A Bismuth-Halide Double Perovskite with Long Carrier Recombination Lifetime for Photovoltaic Applications. *J. Am. Chem. Soc.* **2016**, *138*, 2138−2141.
(67) Connor, B. A.; Leppert, L.; Smith, M. D.; Neaton, J. B.; Karunadasa, H. I. Layered Halide Double Perovskites: Dimensional Reduction of $Cs_2AgBiBr_6$. *J. Am. Chem. Soc.* **2018**, *140*, 5235−5240.
(68) Martín-García, B.; Spirito, D.; Biffi, G.; Artyukhin, S.; Bonaccorso, F.; Krahne, R. Phase Transitions in Low-Dimensional Layered Double Perovskites: The Role of the Organic Moieties. *J. Phys. Chem. Lett.* **2021**, *12*, 280−286.
(69) Do, T. T. H.; Granados del Águila, A.; Zhang, D.; Xing, J.; Liu, S.; Prosnikov, M. A.; Gao, W.; Chang, K.; Christianen, P. C. M.; Xiong, Q. Bright Exciton Fine-Structure in Two-Dimensional Lead Halide Perovskites. *Nano Lett.* **2020**, *20*, 5141−5148.
(70) Wang, J.; Zhu, J.; Jiang, Y.; Li, M.; Yu, K.; Wang, G. P. Observation of Elastic Heterogeneity and Phase Evolution in 2D Layered Perovskites Using Coherent Acoustic Phonons. *Nanophotonics* **2021**, *10*, 4009−4017.
(71) Altaiary, M. M.; Liu, E.; Liang, C.-T.; Hsiao, F.-C.; van Baren, J.; Taniguchi, T.; Watanabe, K.; Gabor, N. M.; Chang, Y.-C.; Lui, C.

H. Electrically Switchable Intervalley Excitons with Strong Two-Phonon Scattering in Bilayer WSe_2. *Nano Lett.* **2022**, *22*, 1829−1835.
(72) Powers, E. R.; Paritmongkol, W.; Yost, D. C.; Lee, W. S.; Grossman, J. C.; Tisdale, W. A. Coherent Exciton-Lattice Dynamics in a 2D Metal Organochalcogenolate Semiconductor. *Matter* **2024**, *7*, 1612−1630.
(73) Avugadda, S. K.; Castelli, A.; Dhanabalan, B.; Fernandez, T.; Silvestri, N.; Collantes, C.; Baranov, D.; Imran, M.; Manna, L.; Pellegrino, T.; Arciniegas, M. P. Highly Emitting Perovskite Nanocrystals with 2-Year Stability in Water through an Automated Polymer Encapsulation for Bioimaging. *ACS Nano* **2022**, *16*, 13657−13666.
(74) Xu, J.; Chen, H.; Grater, L.; Liu, C.; Yang, Y.; Teale, S.; Maxwell, A.; Mahesh, S.; Wan, H.; Chang, Y.; Chen, B.; Rehl, B.; Park, S. M.; Kanatzidis, M. G.; Sargent, E. H. Anion Optimization for Bifunctional Surface Passivation in Perovskite Solar Cells. *Nat. Mater.* **2023**, *22*, 1507−1514.
(75) Hu, W.; Zhang, L. High-Throughput Calculation and Machine Learning of Two-Dimensional Halide Perovskite Materials: Formation Energy and Band Gap. *Mater. Today Commun.* **2023**, *35*, No. 105841.
(76) Wu, Y.; Wang, C.-F.; Ju, M.-G.; Jia, Q.; Zhou, Q.; Lu, S.; Gao, X.; Zhang, Y.; Wang, J. Universal Machine Learning Aided Synthesis Approach of Two-Dimensional Perovskites in a Typical Laboratory. *Nat. Commun.* **2024**, *15*, 138.
(77) Alias, M. S.; Dursun, I.; Saidaminov, M. I.; Diallo, E. M.; Mishra, P.; Ng, T. K.; Bakr, O. M.; Ooi, B. S. Optical Constants of $CH_3NH_3PbBr_3$ Perovskite Thin Films Measured by Spectroscopic Ellipsometry. *Opt. Express* **2016**, *24*, 16586−16594.
(78) Werner, J.; Nogay, G.; Sahli, F.; Yang, T. C.-J.; Bräuninger, M.; Christmann, G.; Walter, A.; Kamino, B. A.; Fiala, P.; Löper, P.; Nicolay, S.; Jeangros, Q.; Niesen, B.; Ballif, C. Complex Refractive Indices of Cesium−Formamidinium-Based Mixed-Halide Perovskites with Optical Band Gaps from 1.5 to 1.8 eV. *ACS Energy Lett.* **2018**, *3*, 742−747.
(79) Song, B.; Hou, J.; Wang, H.; Sidhik, S.; Miao, J.; Gu, H.; Zhang, H.; Liu, S.; Fakhraai, Z.; Even, J.; Blancon, J.-C.; Mohite, A. D.; Jariwala, D. Determination of Dielectric Functions and Exciton Oscillator Strength of Two-Dimensional Hybrid Perovskites. *ACS Mater. Lett.* **2021**, *3*, 148−159.
(80) Anantharaman, S. B.; Lynch, J.; Stevens, C. E.; Munley, C.; Li, C.; Hou, J.; Zhang, H.; Torma, A.; Darlington, T.; Coen, F.; Li, K.; Majumdar, A.; Schuck, P. J.; Mohite, A.; Harutyunyan, H.; Hendrickson, J. R.; Jariwala, D. Dynamics of Self-Hybridized Exciton−Polaritons in 2D Halide Perovskites. *Light: Sci. Appl.* **2024**, *13*, 1.
(81) Zhang, X.; Shi, H.; Dai, H.; Zhang, X.; Sun, X. W.; Zhang, Z. Exciton-Polariton Properties in Planar Microcavity of Millimeter-Sized Two-Dimensional Perovskite Sheet. *ACS Appl. Mater. Interfaces* **2020**, *12*, 5081−5089.

https://doi.org/10.1021/acs.accounts.4c00259
Acc. Chem. Res. 2024, 57, 2476−2489